# The absorption spectrum and absolute absorption cross sections of acetylperoxy radicals, CH3C(O)O2 in the near IR

Michael Rolletter, Emmanuel Assaf, Mohamed Assali, Hendrik Fuchs, Christa Fittschen

Journal of Quantitative Spectroscopy & Radiative Transfer 245 (2020) 106877

Contents lists available at ScienceDirect

Journal of Quantitative Spectroscopy & Radiative Transfer

journal homepage: www.elsevier.com/locate/jqsrt

# The absorption spectrum and absolute absorption cross sections of acetylperoxy radicals, $CH_3C(O)O_2$ in the near IR

Michael Rolletter[a], Emmanuel Assaf[b,#], Mohamed Assali[b], Hendrik Fuchs[a,*], Christa Fittschen[b,*]

[a] Institute of Energy and Climate Research, IEK-8: Troposphere, Forschungszentrum Jülich GmbH, D-52428 Jülich, Germany
[b] Université Lille, CNRS, UMR 8522 - PC2A - Physicochimie des Processus de Combustion et de l'Atmosphère, F-59000 Lille, France

ARTICLE INFO

*Article history:*
Received 11 December 2019
Revised 31 January 2020
Accepted 31 January 2020
Available online 3 February 2020

ABSTRACT

The $\tilde{A}$-$\tilde{X}$ electronic transition of acetylperoxy radicals ($CH_3C(O)O_2$) in the near-infrared was measured at 67hPa synthetic air in the spectral ranges from 6094 $cm^{-1}$ to 6180 $cm^{-1}$ and 6420 $cm^{-1}$ to 6600 $cm^{-1}$. $CH_3C(O)O_2$ radicals were generated by the pulsed photolysis of a acetaldehyde/$Cl_2$/$O_2$ mixture at 351 nm and subsequently measured by time-resolved continuous-wave cavity ring-down spectroscopy (cw-CRDS). The absorption cross sections of eight discrete absorption lines were determined relative to the absorption cross section of $HO_2$, which has previously been reported. The strongest absorption cross section was found at 6510.73 $cm^{-1}$ and was determined to be $(4.9 \pm 2.5) \times 10^{-20}$ $cm^2$.



## 1. Introduction

In the troposphere, the oxidation of volatile organic compounds (VOCs) is mainly driven by hydroxyl (OH) radicals and leads to the formation of organic peroxy radicals ($RO_2$). The fate of these $RO_2$ radicals depends on the chemical composition of the environment. In a polluted atmosphere they react mainly with nitric oxide (NO) to form alkoxy radicals or react with nitrogen dioxide ($NO_2$) to form peroxynitrates ($RO_2NO_2$). Subsequent to the reaction with NO, alkoxy radicals react with $O_2$ to form hydroperoxy ($HO_2$) radicals. $HO_2$ radicals further oxidize NO to $NO_2$ and regenerate OH closing the quasi-catalytic cycle. The photolysis of produced $NO_2$ is the only relevant chemical source of tropospheric ozone. In clean environments with low $NO_x$ ($NO_x = NO + NO_2$) concentrations, the dominant loss of $RO_2$ is due to its reaction with $HO_2$ forming hydroperoxides ROOH and terminating the radical reaction chain. In addition, $RO_2$ radicals can react either with other $RO_2$ as self- ($RO_2 + RO_2$) or cross-reaction ($RO_2 + R'O_2$) or with OH radicals ($RO_2 + OH$) [1–3].

The majority of emitted biogenic non methane hydrocarbons are isoprene (53%) and monoterpene species (16%) [4]. The photooxidation of these highly abundant compounds and their oxidation products form among other products also significant amounts of acetylperoxy radicals ($CH_3C(O)O_2$). In the reaction with $NO_2$, $CH_3C(O)O_2$ form peroxyacetyl nitrate (PAN) which is a toxic secondary air pollutant. In addition, PAN acts as the principal tropospheric reservoir species for $NO_x$ [5]. The only relevant source in the troposphere is this photochemical process, so that PAN is an indicator for photochemical oxidation. Its relatively long atmospheric lifetime of approximately two weeks allows for transport over long distances.

Model calculations of measured radical concentrations in different field studies underestimate $HO_x$ ($HO_x = OH + HO_2$) radical concentrations in remote regions with high emissions of VOCs from biogenic sources [6–9]. Because acetylperoxy radicals are formed from biogenic precursors and serve as source for $HO_2$, understanding of its properties is of importance.

Recent studies show that the $CH_3C(O)O_2 + HO_2$ reaction, which is the most important tropospheric reaction in regions that are dominated by biogenic emissions (low NO emissions), does not only lead to radical chain terminating products (R1, R2), but can also regenerate OH (R3) [10–12]:

$$CH_3C(O)O_2 + HO_2 \rightarrow CH_3C(O)OOH + O_2 \quad (R1)$$

$$\rightarrow CH_3C(O)OH + O_3 \quad (R2)$$

$$\rightarrow CH_3C(O)O + OH + O_2 \quad (R3)$$

* Corresponding authors.
*E-mail addresses:* h.fuchs@fz-juelich.de (H. Fuchs), christa.fittschen@univ-lille.fr (C. Fittschen).
# now at Earth System Research Laboratory, Chemical Sciences Division, National Oceanic and Atmospheric Administration, Boulder, Colorado 80305, United States

https://doi.org/10.1016/j.jqsrt.2020.106877

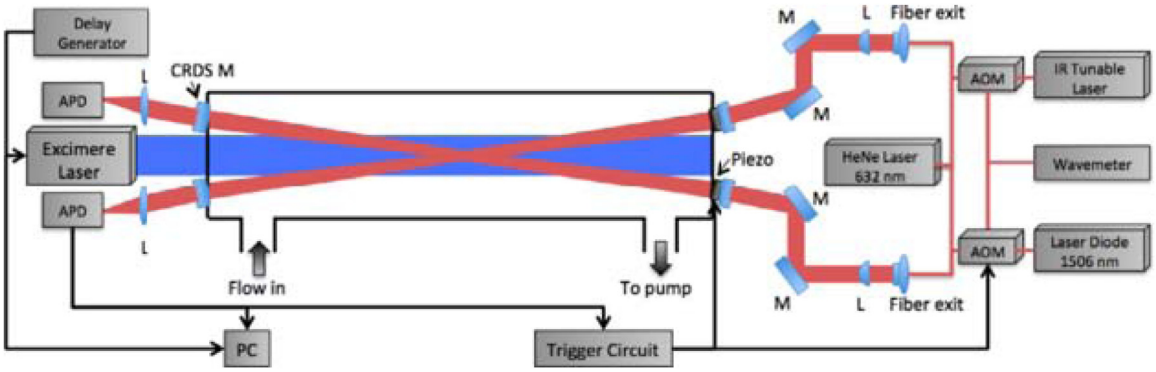


**Fig. 1.** Schematic view of the used experimental setup: AOM, Acousto-Optic Modulator; APD, Avalanche Photo Diode; M, Mirror; L, Lens. Both cw-CRDS systems are equipped with identical trigger circuits and data acquisition systems.

This additional OH radical regeneration could improve the model-measurement agreement in low $NO_x$ environments with high VOC emission rates.

For an accurate understanding of the $CH_3C(O)O_2 + HO_2$ reaction, it is necessary to understand the secondary chemistry. For example, the $CH_3C(O)O_2$ self-reaction (R4) competes with the reaction with $HO_2$, forming the same product $CH_3C(O)O$ as (R3) making it hard to distinguish between both reactions.

$$2\ CH_3(O)O_2 \rightarrow 2\ CH_3C(O)O + O_2 \quad (R4)$$

In addition, reaction rate constants of the self-reaction ($k_4 = 2.9 \times 10^{-12}$ exp(500/T) $cm^3$ $molecule^{-1}$ $s^{-1}$ [13]) and of the reaction with $HO_2$ ($k_{1\text{-}3} = 3.14 \times 10^{-12}$ exp(580/T) $cm^3$ $molecule^{-1}$ $s^{-1}$ [13]) are in the same order of magnitude which makes it complicated to study those reaction kinetics.

The detection of $RO_2$ in previous kinetic laboratory studies was mainly done in the UV region. The spectral overlap of different peroxy species in this region is prone to systematic errors in the quantitative detection [14–18]. Therefore, experiments analysing different $RO_2$ are difficult to evaluate, if they are detected by UV absorption.

Here, we use absorption of $CH_3C(O)O_2$ in the $\tilde{A}$-$\tilde{X}$ electronic transition located in the near infrared region. This results in absorption cross sections that are up to several orders of magnitude smaller compared to values in the UV, but the detection is more selective due to less spectral overlap with formed products. In order to measure these small absorption cross sections, very sensitive detection methods need to be used, in our case continuous wave-Cavity Ring Down Spectroscopy (cw-CRDS). While the relative spectrum has already been measured by Zalyubovsky et al. [19] in a large wavelength range and the absolute absorption cross section of the strongest band at 5582 $cm^{-1}$ has been estimated, we present here the determination of absolute absorption cross sections in two ranges from 6094 $cm^{-1}$ - 6180 $cm^{-1}$ and from 6420 $cm^{-1}$ - 6600 $cm^{-1}$, corresponding to the COO bend and to the OO stretch transition, respectively, relative to the absorption cross section of $HO_2$. These cross sections can be used in future works for the quantitative detection of this radical.

## 2. Experimental

### 2.1. Experimental setup

The setup has been described in detail before [20–23] and is briefly discussed here (Fig. 1).

The setup consisted of a 0.79 m long flow reactor made of stainless steel. The beam of a pulsed excimer laser (Lambda Physik LPX 202i) passed the reactor longitudinally. The flow reactor contained two identical continuous wave cavity ring-down spectroscopy (cw-CRDS) absorption paths, which were installed in a small angle with respect to the photolysis path. An overlap with the photolysis beam of 0.377 m is achieved. Both beam paths were tested for a uniform overlap with the photolysis beam before experiments were done. For this purpose, both cw-CRDS instruments were operated to simultaneously measure $HO_2$ concentrations. Deviations between $HO_2$ concentrations were less than 5% demonstrating that the photolysis laser was very well aligned, *i.e.* both light paths probed a very similar photolysed volume in the reactor. A small helium purge flow prevented the mirrors from being contaminated. For measuring the $CH_3C(O)O_2$ spectrum, a tunable laser source (Agilent 81680A) was coupled into one of the cavities by systems of lenses and mirrors. On the other path, a DFB laser was coupled into the cavity for the detection of $HO_2$ radicals during the calibration measurements. The calibration of the acetylperoxy absorption cross section at 6497.94 and 6638.30 $cm^{-1}$ in 67 hPa helium has also been carried out using a DFB laser instead of the Agilent module. Each probe beam passed an acousto-optic modulator (AOM, AAoptoelectronic) to rapidly turn off the 1st order beam once a threshold for light intensity in the cavity was reached, in order to measure the ring-down event. Then, the decay of light intensity was recorded and an exponential fit is applied to retrieve the ring-down time. The absorption coefficient $\alpha$ is derived from Eq. (1).

$$\alpha = [A] * \sigma_A = \frac{R_L}{c}\left(\frac{1}{\tau} - \frac{1}{\tau_0}\right) \quad (1)$$

where $\tau$ is the ring-down time with an absorber present; $\tau_0$ is the ring-down time with no absorber present; $\sigma_A$ is the absorption cross section of the absorbing species A; $R_L$ is the ratio between cavity length (79 cm) and effective absorption path (37.7 cm); c is the speed of light. To calculate the absorption cross section it is necessary to know the absorber concentration.

Acetylperoxy radicals were generated by pulsed 351 nm photolysis of acetaldehyde ($CH_3CHO$) / $Cl_2$ / $O_2$ mixtures:

$$Cl_2 + h\nu \rightarrow 2\ Cl \quad (R5)$$

$$CH_3CHO + Cl \rightarrow CH_3CO + HCl \quad (R6)$$

$$CH_3CO + O_2 + M \rightarrow CH_3C(O)O_2 + M \quad (R7)$$

The Cl radical concentration for the measurement of the spectrum was around $1.7 \times 10^{12}$ $cm^{-3}$ and was varied for the calibration measurements between (1 and 8) $\times$ $10^{12}$ $cm^{-3}$. Acetaldehyde was prepared as a diluted mixture in a glass bulb. A small flow was added to the mixture through a calibrated flow meter giving a concentration of 2.5 $\times$ $10^{14}$ $cm^{-3}$. Nearly all experiments were performed in synthetic air, at 298 K and 67 hPa total pressure,

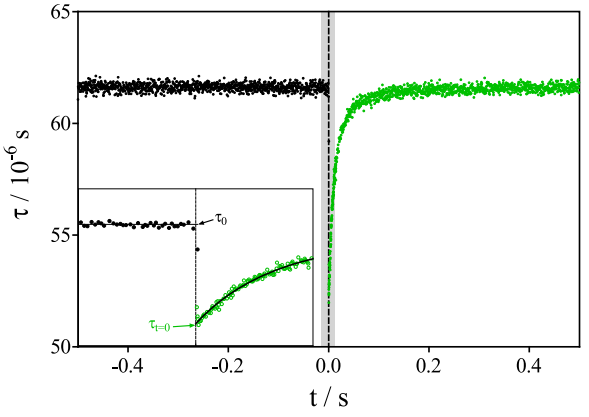


**Fig. 2.** Typical series of ring-down times for $CH_3C(O)O_2$, the insert shows the zoom of the gray-shaded area (+/−15 ms). The dashed line represents the time of the photolysis pulse ($t = 0$ s). Ring-down events before the photolysis pulse (black) are used to determine $\tau_0$, extrapolation to $t = 0$ s of a bi-exponential fit of the ring-down times occurring during the first 50 ms after the photolysis pulse (black line in the insert) are used to determine $\tau$.

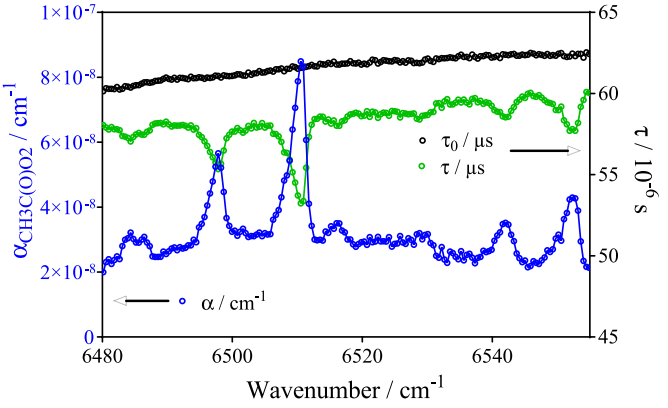


**Fig. 3.** Portion of the relative absorption spectrum: each dot, corresponding to one wavelength, is extracted from a kinetic decay such as shown in Fig. 2. Black dots represent baseline ($\tau_0$), green dots obtained from extrapolation of bi-exponential fitting such as shown in Fig. 2 ($\tau_{t=0}$), blue dots ($\alpha$) obtained by applying equation (Eq. (1)).

the absorption cross sections at 6697.94 and 6638.30 $cm^{-1}$ were also determined at 67 hPa helium. $N_2$ (Praxair, 4.5), He (Praxair 4.5) and $O_2$ (Praxair, 4.5) were used without further purification. All gas flows were controlled by calibrated mass flow controllers (Bronkhorst, Tylan).

### 2.2. Absorption spectra measurements

The procedure to measure absorption spectra has been described before [24,25] and is only briefly discussed here. The spectrum was measured with a point spacing of 0.1 $cm^{-1}$ for the wavelength range from 6094 - 6180 $cm^{-1}$ and 0.2 $cm^{-1}$ for the wavelength range from 6420 - 6600 $cm^{-1}$, corresponding to the COO bend and the OO stretch, respectively [19]. Both wavelength regions have been sampled by changing incrementally the wavelength of the laser while a constant amount of $CH_3C(O)O_2$ was generated in the reactor.

For each wavelength, a time series of ring-down measurements testing the acetyperoxy radical absorption was recorded. After the data acquisition was triggered ring-down events were usually recorded 0.5 s each before and after the photolysis laser shot which led to the formation of acetylperoxy radicals. A typical trace is shown in Fig. 2, where ring-down times from ring-down events occurring before the photolysis pulse are shown in black, and those after the photolysis pulse are shown in green. The loss of $CH_3C(O)O_2$ radicals is for the first tens of ms mostly due to self-reaction and to the reaction with the radical products of this self-reaction ($CH_3O_2$ and $HO_2$). With decreasing radical concentrations on the longer time scale, diffusion out of the photolysis volume becomes the major loss process. To derive the absorbance of the initially produced acetylperoxy radicals, the time-resolved series of ring-down events was extrapolated to the moment of the photolysis pulse (t = 0 s). Different fitting procedures were tested, and it turned out that a bi-exponentiel fit over the first 50 ms following the photolysis pulse reproduced the data very well and allowed a reliable extrapolation to t = 0 s. However, it has to be kept in mind that the decay of the $CH_3C(O)O_2$ concentration is due to a complex reaction scheme, and the decay constants from the fit have no physical meaning. The quality of the fit is shown as a black line in the insert of Fig. 2. $\tau_0$, that is required to calculate the absorbance (Eq. (1)), was derived from the average of all detected ring-down events that occurred before the photolysis pulse when no $CH_3C(O)O_2$ was present. The ring-down events are randomly distributed in time at each photolysis shot because of the random nature of when exactly an efficient coupling of the laser into the cavity was achieved. Ring-down events were therefore accumulated over several laser pulses (10 – 20 generally) to get a better coverage of the whole time range.

## 3. Results and discussion

A portion of the relative absorption spectrum of the OO stretch region is shown in Fig. 3. For each wavenumber, measurements were evaluated as shown in Fig. 2. Ring-down times extrapolated to t = 0 s (green) and $\tau_0$ as the average of all ring-down times before the photolysis pulse (black) are shown for each wavenumber in Fig. 3. The absorption coefficients (blue) are calculated by applying equation (Eq. (1)) to each data pair $\tau$ and $\tau_0$.

In order to convert the absorption coefficient $\alpha$ into absolute cross sections $\sigma$, the knowledge of the exact $CH_3C(O)O_2$ concentration is necessary. Therefore, a series of experiments was conducted to quantify the initial amount of radicals. This was achieved by quantitatively converting all Cl-atoms to $HO_2$ radicals, which can be reliably measured by cw-CRDS on a strong absorption line at 6638.205 $cm^{-1}$ [23,26–29]. The measurement of the $HO_2$ absorption cross section is based on the measurement of $HO_2$ decays during self-reaction, which allows for retrieval of the initial concentration, and thus the absorption cross section, if the rate constant is known. While the uncertainty of the measured $HO_2$ decays itself is small (<10%), the uncertainty of the rate constant is currently recommended by the IUPAC committee to ±40%. This same uncertainty has to be considered for the absorption cross sections obtained in this work, as they are measured relative to the $HO_2$ absorption cross section. The quantitative conversion of Cl-atoms to $HO_2$ is done by photolysing a $Cl_2$ / methanol ($CH_3OH$) mixture:

$$Cl + CH_3OH \rightarrow HCl + CH_2OH \quad (R9)$$

$$CH_2OH + O_2 \rightarrow CH_2O + HO_2 \quad (R10)$$

Then, $CH_3OH$ is substituted by $CH_3CHO$ to form $CH_3C(O)O_2$ following reactions (R11) and (R12), while keeping conditions for the generation of Cl radicals constant.

$$Cl + CH_3CHO \rightarrow HCl + CH_3CO \quad (R11)$$

$$CH_3CO + O_2 \rightarrow CH_3C(O)O_2 \quad (R12a)$$

Assuming that the concentration of $HO_2$ radicals corresponds to the concentration of Cl atoms, the ratio of absorbance measured

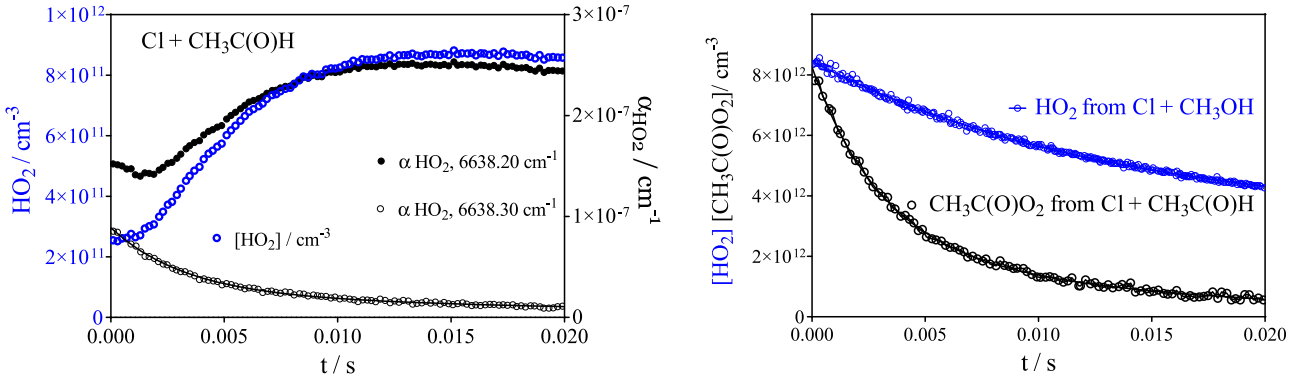


**Fig. 4.** Left plot shows $HO_2$ absorption coefficient online (6638.20 $cm^{-1}$, black dots) and offline (6638.30 $cm^{-1}$, open black symbols, right y-axis apply for both) and $HO_2$ concentration (blue symbols, left y-axis) measured after photolysing a $Cl_2$ / $CH_3CHO$ / $O_2$ mixture. Right graph shows the $HO_2$ concentration from the photolysis of $Cl_2$ / $CH_3OH$ / $O_2$ mixture (blue symbols) and the $CH_3C(O)O_2$ concentration time profile from the photolysis of the $Cl_2$ / $CH_3CHO$/ $O_2$ mixture (black symbols). Both experiments used the same $Cl_2$ concentration.

for $CH_3C(O)O_2$ and $HO_2$ can be used to calculate the $CH_3C(O)O_2$ absorption cross section relative to the well known $HO_2$ absorption cross section according to:

$$\sigma_{CH_3C(O)O_2} = \alpha_{CH_3C(O)O_2} \frac{\sigma_{HO_2}}{\alpha_{HO_2}} \quad (2)$$

However, the assumption does not entirely apply, because the reaction of $CH_3CO + O_2$ leads also to the formation of some OH radicals, the yield depending on pressure and nature of the $CH_3CO$ precursor [30–32]. An OH yield of 0.25 is expected in nitrogen at 67 hPa [30].

$$CH_3CO + O_2 \rightarrow OH + \text{products} \quad (R12b)$$

OH radical concentrations can in principle be measured by cw-CRDS in the experimental set-up [33]. However, concentrations in these experiments were below the limit of detection likely due to the fast reaction with acetaldehyde [13]:

$$CH_3CHO + OH \rightarrow CH_3CO + H_2O \quad (R13)$$

Because under our experimental conditions ($[CH_3CHO] = 2.5 \times 10^{14}$ $cm^{-3}$), (R13) is leading with $k_{13} = 1.5 \times 10^{-11}$ $cm^3$ $s^{-1}$ to an OH lifetime of 250 µs, and can thus, in absence of other potential reaction partners, be considered as the nearly exclusive fate of OH radicals. And because (R13) leads to formation of another $CH_3CO$ radical, this reaction does not introduce an error in the calculation of the absorption cross section using equation (Eq. (2)).

However, it was observed in our experiments that small amounts of $HO_2$ radicals are formed immediately from the initial reaction of $CH_3CHO + Cl$. Radical concentrations measured in a typical experiment are shown in Fig. 4: the left graph shows the $HO_2$ signal obtained from photolysis of $Cl_2$ / $CH_3CHO$ / $O_2$ mixture. Because $CH_3C(O)O_2$ has a broad absorption spectrum [19], it still absorbs in the wavelength range where $HO_2$ is detected (6638.2 $cm^{-1}$). Therefore, absolute $HO_2$ concentrations (blue symbols) are obtained from the difference of the online (6638.2 $cm^{-1}$) and the offline (6638.3 $cm^{-1}$) absorption signal. It can be seen that the $HO_2$ concentration immediately after the photolysis pulse is not zero. The blue symbols on the right graph show the $HO_2$ concentration time profile under the same conditions, but with $CH_3OH$ instead of $CH_3CHO$. Comparing the $HO_2$ concentrations measured from methanol mixtures ($[HO_2]_{CH_3OH}$) and acetaldehyde mixtures ($[HO_2]_{CH_3C(H)O}$) shows that around 3% of the Cl-atoms are converted to $HO_2$ ($\delta_{HO_2}$) in the presence of $CH_3CHO$.

**Table 1**
Absorption coefficient $\alpha$ for $CH_3C(O)O_2$ from the measurement of the full spectrum for eight wavenumbers (marked by lines in the full spectrum of Fig. 6) and absorption cross sections $\sigma$ for the same lines, determined relative to the $HO_2$ cross section at 67 hPa $N_2$ and for two wavenumbers at 67 hPa helium.

| Wavenumber / $cm^{-1}$ | $\alpha$ / $10^{-8}$ $cm^{-1}$ | $\sigma$ / $10^{-20}$ $cm^2$ |
|---|---|---|
| 6121.08 | 5.65 ± 0.28 | 3.4 ± 1.7 |
| 6164.75 | 2.75 ± 0.14 | 1.7 ± 0.8 |
| 6108.74 | 4.01 ± 0.20 | 2.2 ± 1.1 |
| 6114.53 | 1.59 ± 0.08 | 0.9 ± 0.5 |
| 6497.94 | 5.35 ± 0.27 | 3.2 ± 1.6 |
| 6697.94 (helium) | | 3.3 ± 1.7 |
| 6502.80 | 3.03 ± 0.15 | 1.7 ± 0.9 |
| 6552.76 | 4.29 ± 0.21 | 2.5 ± 1.3 |
| 6510.74 | 8.49 ± 0.42 | 4.9 ± 2.4 |
| 6638.30 (helium) | | 0.8 ± 0.4 |

$$\delta_{HO_2} = \frac{[HO_2]_{CH_3CHO}}{[HO_2]_{CH_3OH}} \quad (3)$$

This small correction of the initial $CH_3C(O)O_2$ concentration was taken into account when converting the absorption coefficient of $CH_3C(O)O_2$ into absorption cross sections:

$$\sigma_{CH_3C(O)O_2} = \alpha_{CH_3C(O)O_2} \frac{\sigma_{HO_2}}{\alpha_{HO_2}} \times \frac{1}{(1 - \delta_{HO_2})} \quad (4)$$

The origin of this rapid $HO_2$ formation is not clear, but is formed possibly through the reaction

$$CH_3CO + O_2 \rightarrow CH_2CO + HO_2 \quad (R12c)$$

Such a rapid $HO_2$ formation with similar yields had already been observed by Morajkar et al. [34]. with a yield of around 7%, independent of pressure between 10 and 90 Torr helium, following the 248 nm photolysis of $CH_3CHO$, and also by Hui et al. [35]. with a yield of 2–3% following the reaction of Cl-atoms with $CH_3CHO$ at 100 Torr $N_2$. $HO_2$ concentrations at 67 hPa $N_2$ have been calculated using an absorption cross section of $\sigma_{HO_2,6638.20cm\text{-}1} = 2.01 \times 10^{-19}$ $cm^2$, obtained from the empirical expression of Assaf et al. [27].

This way, absorption cross sections $\sigma$ were measured for 8 wavenumbers in synthetic air and for 2 wavenumbers in helium, given in Table 1 together with the absorption coefficients $\alpha$ for the same wavelengths in synthetic air, such as found during the measurement of the full spectrum. Also given in Table 1 are the absorption cross sections for two wavenumbers, obtained in 67 hPa

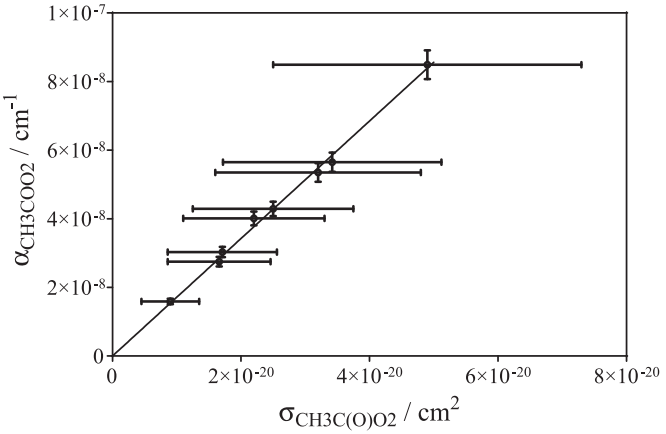


**Fig. 5.** Absorption coefficients $\alpha$ as a function of the absorption cross sections $\sigma$ from Table 1. Error bars are statistical for absorption coefficients $\alpha$ (5%), and an uncertainty of 45% is added for the absorption cross section $\sigma$, taking into account the uncertainty in the absorption cross section for $HO_2$.

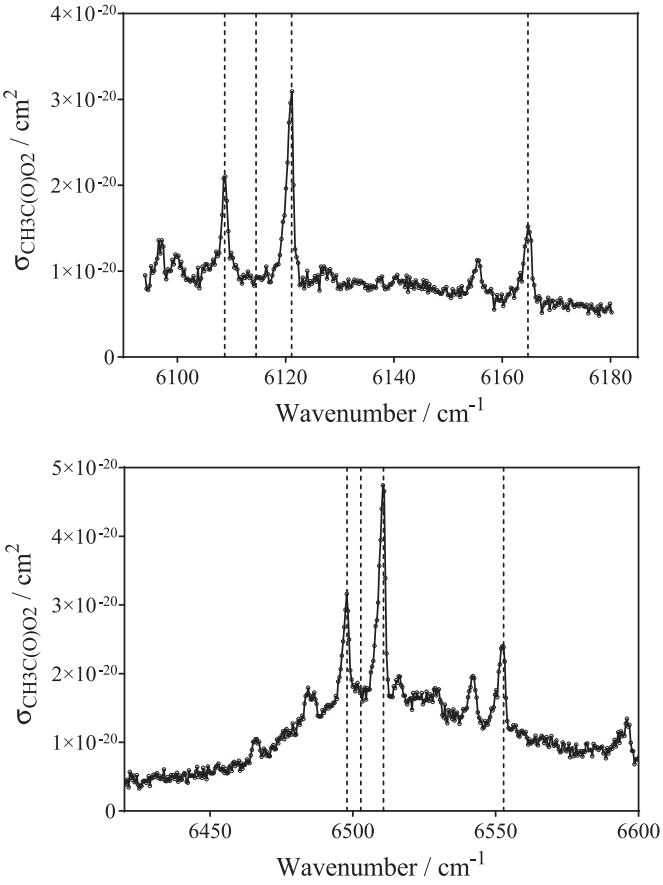


**Fig. 6.** Absolute absorption spectrum of $CH_3C(O)O_2$. Vertical lines indicate the wavelengths where absolute absorption cross sections have been determined relative to the absorption cross section of $HO_2$ (see Table 1). The data can be downloaded as supplementary data.

helium: 6697.94 $cm^{-1}$ corresponds to one peak of the OO-stretch transition band, while 6638.30 $cm^{-1}$ corresponds to the wavenumber that we commonly use for the measurement of the $HO_2$-offline signal, i.e. the open circles in Fig. 4. The error bars of the absorption coefficients $\alpha$ are statistical only and are given with ±5%, obtained from the 95% confidence interval of the extrapolation of the bi-exponential fit to $t = 0$ s (black curve in the insert of Fig. 2, typically below 4%) as well as the $\tau_0$ (average of all ring down events before the photolysis pulse: typically less than 1%). The error bars for the absorption cross sections are given with ±50% and are composed of twice the uncertainty of extrapolating $\alpha$ to $t = 0$ s (once for $\alpha_{CH_3C(O)O_2}$ and once for $\alpha_{HO_2}$) and the 40% uncertainty given by the IUPAC committee [36] for the rate constant of the $HO_2$ self-reaction, that was used to determine the absorption cross section of $HO_2$.

In Fig. 5 the absorption coefficients are plotted for all eight wavenumbers as a function of the absorption cross sections $\sigma$. A good linearity is found, assuring that the $CH_3C(O)O_2$ concentration was stable during the measurement of the full spectrum.

The slope from the linear regression of Fig. 5 leads to the concentration of $CH_3C(O)O_2$ radicals that was generated during the measurement of the full spectrum: $1.7 \times 10^{12}$ $cm^{-3}$. This value was used for the conversion of the absorption coefficients from the relative spectra (blue line in Fig. 3) of the two wavelength ranges into absolute absorption cross sections, shown in Fig. 6. A comparison with a previously published spectrum [19] shows an excellent agreement of the positions and relative intensities of the different absorption maxima.

Zalyubovsky et al. [19] determined an absorption cross section of $\sigma = (1 \pm 0.5) \times 10^{-19}$ $cm^2$ at 5582.5 $cm^{-1}$. This is consistent with our absorption cross section of $(4.9 \pm 2.4) \times 10^{-20}$ $cm^2$ at the absorption maximum 6510.71 $cm^{-1}$, which has in the spectrum of Zalyubovsky et al. a relative intensity of approximately a factor 2 less than the absorption maximum at 5582.5 $cm^{-1}$.

The results obtained in this work will be used in future studies on the reaction kinetics of $CH_3C(O)O_2$ radicals. Depending on the quality of alignment, cleanliness of mirrors, etc. a decrease of the ring-down time of $\Delta\tau = 0.5$ µs on a typical $\tau_0 = 50$ µs can be achieved in time-resolved experiments, leading to a limit of detection below $[CH_3C(O)O_2] = 4 \times 10^{11}$ $cm^{-3}$, making this technique more sensitive than typical UV-absorption measurements. And even though the spectrum features a rather broad background, *i.e.* lacks the high selectivity that can be achieved for $HO_2$ or OH measurements, its main absorption peaks are red-shifted compared to other small peroxy radicals such as $HO_2$, $CH_3O_2$ [24,37,38], $C_2H_5O_2$ [37] and should thus allow a selective detection for measuring the rate constants and branching ratios of self- and cross-reactions.

## 4. Conclusion

We measured the $CH_3C(O)O_2$ absorption spectrum in the ranges from 6094 $cm^{-1}$ - 6180 $cm^{-1}$ and 6420 $cm^{-1}$ - 6600 $cm^{-1}$. Measurements were performed in 67 hPa synthetic air or helium total pressure. Radicals were generated by the pulsed photolysis of acetaldehyde / $Cl_2$ / $O_2$ mixtures at 351 nm.

Some large peaks on top of a broad absorption spectrum were obtained, in good agreement with an earlier measurement by Zalyubovsky et al. [19]. Absolute absorption cross sections were measured for eight different wavelengths and are in good agreement relative to the only available measurement by Zalyubovsky et al. [19] performed at a lower wavenumber.

## Declaration of Competing Interest

The authors declare that they have no known competing financial interests or personal relationships that could have appeared to influence the work reported in this paper.

## CRediT authorship contribution statement

**Michael Rolletter:** Data curation, Writing - original draft. **Emmanuel Assaf:** Investigation, Data curation, Resources.

**Mohamed Assali:** Investigation, Data curation. **Hendrik Fuchs:** Conceptualization, Writing - review & editing, Supervision, Funding acquisition. **Christa Fittschen:** Conceptualization, Writing - original draft, Supervision, Project administration, Funding acquisition.

## Acknowledgments

This project was supported by the French ANR agency under contract No. ANR-11-Labx-0005-01 CaPPA (Chemical and Physical Properties of the Atmosphere), the Région Hauts-de-France, the Ministère de l'Enseignement Supérieur et de la Recherche (CPER Climibio) and the European Fund for Regional Economic Development. This project has received funding from the European Research Council (ERC) under the European Union's Horizon 2020 research and innovation program (SARLEP grant agreement No. 681529) and from the exchange program of the Deutscher Akademischer Austauschdienst (DAAD) (project number 57316518) and PHC Procope project no. 37666WA.

## Supplementary materials

Supplementary material associated with this article can be found, in the online version, at doi:10.1016/j.jqsrt.2020.106877.

## References

[1] Orlando JJ, Tyndall GS. Laboratory studies of organic peroxy radical chemistry: an overview with emphasis on recent issues of atmospheric significance. Chem Soc Rev 2012;41:6294–317.
[2] Fittschen C. The reaction of peroxy radicals with OH radicals. Chem Phys Lett 2019;725:102–8.
[3] Assaf E, Song B, Tomas A, Schoemaecker C, Fittschen C. Rate constant of the reaction between $CH_3O_2$ radicals and OH radicals revisited. J Phys Chem A 2016;120:8923–32.
[4] Guenther AB, Jiang X, Heald CL, Sakulyanontvittaya T, Duhl T, Emmons LK, et al. The model of emissions of gases and aerosols from nature version 2.1 (MEGAN2. 1): an extended and updated framework for modeling biogenic emissions. Geosci Model Dev 2012;5:1471–92.
[5] Fischer EV, Jacob DJ, Yantosca RM, Sulprizio MP, Millet DB, Mao J, et al. Atmospheric peroxyacetyl nitrate (PAN): a global budget and source attribution. Atmos Chem Phys 2014;14:2679–98.
[6] Tan D, Faloona I, Simpas JB, Brune W, Shepson PB, Couch TL, et al. $HO_x$ budgets in a deciduous forest: results from the PROPHET summer 1998 campaign. J Geophys Res Atmos 2001;106:24407–27.
[7] Lelieveld J, Butler TM, Crowley JN, Dillon TJ, Fischer H, Ganzeveld L, et al. Atmospheric oxidation capacity sustained by a tropical forest. Nature 2008;452:737–40.
[8] Hofzumahaus A, Rohrer F, Lu K, Bohn B, Brauers T, Chang CC, et al. Amplified trace gas removal in the troposphere. Science 2009;324:1702–4.
[9] Wolfe GM, Thornton JA, Bouvier-Brown NC, Goldstein AH, Park JH, McKay M, et al. The Chemistry of Atmosphere-Forest Exchange (CAFE) model - Part 2: application to BEARPEX-2007 observations. Atmos Chem Phys 2011;11:1269–94.
[10] Hasson AS, Tyndall GS, Orlando JJ. A product yield study of the reaction of $HO_2$ radicals with ethyl peroxy ($C_2H_5O_2$), acetyl peroxy ($CH_3C(O)O_2$), and acetonyl peroxy ($CH_3C(O)CH_2O_2$) radicals. J Phys Chem A 2004;108:5979–89.
[11] Winiberg FAF, Dillon TJ, Orr SC, Groß CBM, Bejan I, Brumby CA, et al. Direct measurements of oh and other product yields from the $HO_2 + CH_3C(O)O_2$ reaction. Atmos Chem Phys 2016;16:4023–42.
[12] Hui AO, Fradet M, Okumura M, Sander SP. Temperature dependence study of the kinetics and product yields of the $HO_2 + CH_3C(O)O_2$ reaction by direct detection of OH and $HO_2$ radicals using 2f-IR wavelength modulation spectroscopy. J Phys Chem A 2019;123:3655–71.
[13] Atkinson R, Baulch DL, Cox RA, Crowley JN, Hampson RF, Hynes RG, et al. Evaluated kinetic and photochemical data for atmospheric chemistry: volume ii - gas phase reactions of organic species. Atmos Chem Phys 2006;6:3625–4055.
[14] Addison MC, Burrows JP, Cox RA, Patrick R. Absorption-Spectrum and kinetics of the acetylperoxy radical. Chem Phys Lett 1980;73:283–7.
[15] Moortgat G, Veyret B, Lesclaux R. Absorption-Spectrum and kinetics of reactions of the acetylperoxy radical. J Phys Chem 1989;93:2362–8.
[16] Lightfoot P.D., Cox R.A., Crowley J.N., Destriau M., Hayman G.D., Jenkin M.E., et al. Organic peroxy-radicals - Kinetics, spectroscopy and tropospheric chemistry. atmospheric environment part a-General topics. 1992;26:1805–961.
[17] Roehl CM, Bauer D, Moortgat GK. Absorption spectrum and kinetics of the acetylperoxy radical. J Phys Chem 1996;100:4038–47.
[18] Maricq MM, Szente JJ. The $CH_3C(O)O_2$ radical. its uv spectrum, self-reaction kinetics, and reaction with $CH_3O_2$. J Phys Chem 1996;100:4507–13.
[19] Zalyubovsky SJ, Glover BG, Miller TA. Cavity ringdown spectroscopy of the $\tilde{A}-\tilde{X}$ electronic transition of the $CH_3C(O)O_2$ radical. J Phys Chem A 2003;107:7704–12.
[20] Thiebaud J, Fittschen C. Near infrared cw-CRDS coupled to laser photolysis: spectroscopy and kinetics of the $HO_2$ radical. Appl Phys B 2006;85:383–9.
[21] Parker AE, Jain C, Schoemaecker C, Szriftgiser P, Votava O, Fittschen C. Simultaneous, time-resolved measurements of OH and $HO_2$ radicals by coupling of high repetition rate lif and cw-CRDS techniques to a laser photolysis reactor and its application to the photolysis of $H_2O_2$. Appl Phys B 2011;103:725–33.
[22] Votava O, Mašát M, Parker AE, Jain C, Fittschen C. Microcontroller based resonance tracking unit for time resolved continuous wave cavity-ringdown spectroscopy measurements. Rev Sci Instrum 2012;83:043110.
[23] Assaf E, Asvany O, Votava O, Batut S, Schoemaecker C, Fittschen C. Measurement of line strengths in the $\tilde{A}$ $2A' \leftarrow x$ $2A''$ transition of $HO_2$ and $DO_2$. J Quant Spectrosc Radiat Transfer 2017;201:161–70.
[24] Faragó EP, Viskolcz B, Schoemaecker C, Fittschen C. Absorption spectrum and absolute absorption cross sections of $CH_3O_2$ radicals and CH3I molecules in the wavelength range 7473–7497 cm–1. J Phys Chem A 2013;117:12802–11.
[25] Jain C, Morajkar P, Schoemaecker C, Viskolcz B, Fittschen C. Measurement of absolute absorption cross sections for nitrous acid (HONO) in the near-infrared region by the continuous wave cavity ring-down spectroscopy (cw-CRDS) technique coupled to laser photolysis. J Phys Chem A 2011;115:10720–8.
[26] Thiebaud J, Crunaire S, Fittschen C. Measurements of line strengths in the $2\nu 1$ band of the $HO_2$ radical using laser photolysis/continuous wave cavity ring–down spectroscopy (cw-CRDS). J Phys Chem A 2007;111:6959–66.
[27] Assaf E, Liu L, Schoemaecker C, Fittschen C. Absorption spectrum and absorption cross sections of the $2\nu_1$ band of $HO_2$ between 20 and 760Torr air in the range 6636 and 6639 $cm^{-1}$. J Quant Spectrosc Radiat Transf 2018;211:107–14.
[28] Onel L, Brennan A, Gianella M, Ronnie G, Lawry Aguila A, Hancock G, et al. An intercomparison of $HO_2$ measurements by fluorescence assay by gas expansion and cavity ring-down spectroscopy within HIRAC (Highly instrumented reactor for atmospheric chemistry). Atmos Meas Tech 2017;10:4877–94.
[29] Tang Y, Tyndall GS, Orlando JJ. Spectroscopic and kinetic properties of $HO_2$ radicals and the enhancement of the $HO_2$ self reaction by $CH_3OH$ and $H_2O$. J Phys Chem A 2010;114:369–78.
[30] Groß CBM, Dillon TJ, Crowley JN. Pressure dependent oh yields in the reactions of $CH_3CO$ and $HOCH_2CO$ with $O_2$. Phys Chem Chem Phys 2014;16:10990–8.
[31] Carr SA, Baeza-Romero MT, Blitz MA, Pilling MJ, Heard DE, Seakins PW. OH yields from the $CH_3CO+O_2$ reaction using an internal standard. Chem Phys Lett 2007;445:108–12.
[32] Devolder P, Dusanter S, Lemoine B, Fittschen C. About the co-product of the OH radical in the reaction of acetyl with $O_2$ below atmospheric pressure. Chem Phys Lett. 2006;417:154–8.
[33] Assaf E, Fittschen C. Cross section of oh radical overtone transition near 7028 $cm^{-1}$ and measurement of the rate constant of the reaction of OH with $HO_2$ radicals. J Phys Chem A 2016;120:7051–9.
[34] Morajkar P, Bossolasco A, Schoemaecker C, Fittschen C. Photolysis of $CH_3CHO$ at 248 nm: evidence of triple fragmentation from primary quantum yield of $CH_3$ and HCO radicals and h atoms. J Chem Phys 2014;140:214308.
[35] Hui AO, Fradet M, Okumura M, Sander SP. Temperature dependence study of the kinetics and product yields of the $HO_2 + CH_3C(O)O_2$ reaction by direct detection of oh and $HO_2$ radicals using 2f-IR wavelength modulation spectroscopy. J Phys Chem A 2019;123:3655–71.
[36] Atkinson R, Baulch DL, Cox RA, Crowley JN, Hampson RF, Hynes RG, et al. Evaluated kinetic and photochemical data for atmospheric chemistry: volume 1 – Gas Phase reactions of $O_x$, $HO_x$, $NO_x$, and $SO_x$, species, IUPAC task group on atmospheric chemical kinetic data evaluation. Atmos Chem Phys. 2004;2(4):1461–738. http://iupac.pole-ether.fr.
[37] Atkinson DB, Hudgens JW. Chemical kinetic studies using ultraviolet cavity ring-down spectroscopic detection: self-reaction of ethyl and ethylperoxy radicals and the reaction $O_2 + C_2H_5 \rightarrow C_2H_5O_2$. J Phys Chem A 1997;101:3901–9.
[38] Chung C-Y, Cheng C-W, Lee Y-P, Liao H-Y, Sharp EN, Rupper P, et al. Rovibronic bands of the $\tilde{A} \leftarrow \tilde{X}$ transition of $CH_3OO$ and $CD_3OO$ detected with cavity ring-down absorption near 1.2–1.4μm. J Chem Phys 2007;127:044311.